Available online at www.sciencedirect.com
ScienceDirect
Polymer 48 (2007) 1297–1305
polymer
www.elsevier.com/locate/polymer

Quantitative probing the interfacial structure of TPO/CPO blends by transmission electron microscopy via EDX

Zhihui Yin [a], Jian Yang [a], Neil Coombs [a], Mitchell A. Winnik [a,*], Rose A. Ryntz [b], Philip V. Yaneff [c]

[a] *Department of Chemistry, University of Toronto, 80 St. George Street, Toronto, Ontario, Canada M5S 3H6*
[b] *Visteon Automotive Systems, Dearborn, MI 58121, USA*
[c] *E.I. DuPont Canada, 408 Fairall Street, Ajax, Ontario, Canada L1S 1R6*

Received 8 April 2006; received in revised form 22 December 2006; accepted 2 January 2007
Available online 7 January 2007

Abstract

High-resolution scanning transmission electron microscope (HR STEM) measurements were performed on a thermoplastic polyolefin (TPO) substrate coated with chlorinated polyolefin (CPO). This CPO was a maleated chlorinated polypropylene containing 21.8 wt% Cl. The TPO investigated was a blend of high-modulus isotactic polypropylene (iPP) with a crystalline ethylene–butene copolymer (EB9) containing 9 wt% butene. For these injection-molded samples, examined ca. 10 mm from the mold gate, a stratified morphology found at TPO surface consisting of thin fibers of EB9 trapped in a transcrystalline iPP matrix, with crystalline lamellae propagating from the matrix across the EB9 domains. This structure was unperturbed when the plaques were coated (from tetrahydrofuran solution) with a 5 μm layer of CPO, but underwent changes of increasing severity when subjected either to a dry bake at 120 °C or annealing at 120 °C in the presence of xylene vapor. The interfacial structure between the CPO and the TPO was probed by TEM with energy dispersive X-ray imaging (EDX). The elemental chlorine across the interface gave good fits to a tan *h* function, and the interface thickness increased from 23 ± 2 nm to 28 ± 1 nm upon annealing at 120 °C for 30 min. After annealing in the presence of xylene vapor, this value increased to 50 ± 4 nm. As reference points, we determined an interface thickness of 29 ± 3 nm for the CPO–EB interface and 15 ± 2 nm for the interface between CPO and iPP.

Keywords: Polypropylene blends; TPO; Adhesion promoter

1. Introduction

Thermoplastics olefins (TPOs) are an important class of polymer blend materials for the automotive industry. TPOs are used to fabricate bumpers, fascia, and other exterior and interior trim components. The term TPO refers to a family of polyolefin blends consisting of isotactic polypropylene (iPP) containing various other polyolefins as impact modifiers. Common examples for the impact modifier are ethylene–propylene rubber (EPR) and ethylene–propene–diene monomer (EPDM) polymers of various compositions. Plastic automotive parts, particularly the exterior parts, are painted to increase the longevity of the part and to enhance the cosmetic appearance. Owing to the low surface energy of the TPO substrates, paint does not normally adhere very well to these substrates, and surface modification is needed to improve adhesion. One approach to addressing this problem is to coat the TPO with a polymeric adhesion promoter that serves as an adhesion layer between the substrate and the coating. For example, injection-molded TPO parts are commonly coated with an adhesion promoter consisting of a maleated, chlorinated polypropylene referred to generally as CPO. Although CPO has been used by the automotive industry for many years as the major component of adhesion promoter formulations, we have relatively little fundamental knowledge about the mechanism of adhesion or the nature of the interface between CPO and TPO.

A number of investigations have been reported describing experiments designed to help develop a better understanding

* Corresponding author. Tel.: +1 416 978 6495; fax: +1 416 978 0541.
E-mail address: mwinnik@chem.utoronto.ca (M.A. Winnik).

0032-3861/$ - see front matter © 2007 Elsevier Ltd. All rights reserved.
doi:10.1016/j.polymer.2007.01.004

the nature of the interfacial adhesion of CPO onto TPO [1–9]. It is generally proposed that during the coating of the adhesion promoter and the subsequent baking step, CPO chains diffuse into the TPO substrate and entangle with components of the TPO [1–5]. Most authors believe that the CPO interacts preferentially with the rubber layer of the impact modifier that lies beneath an iPP-rich surface layer. PP has a lower surface energy than the ethylene copolymers used as impact modifiers, so there is good reason to expect that the surface of injection-molded TPO parts will have an iPP-rich surface. There are also strong indications that CPO has a stronger interaction with the rubber phase than with iPP itself. The entanglements between the rubber phase and the CPO are thought to create the physical links that provide adhesion between the CPO and TPO.

It is important to keep in mind that there are many different TPO compositions as well as a variety of different CPOs. The CPOs based on PP differ in chain length, chlorine content, and the amount of succinic anhydride groups introduced through maleation. Within the industry, there is a sense that particular CPOs work best on individual TPO compositions, although we are unaware of any literature documenting these differences. Many of the ideas described above were developed for TPO compositions involving amorphous polymers as the impact modifier. In many of these publications, which one can now think of as exploratory in nature, the details of the TPO and CPO compositions were not reported, and probably were not revealed to the experimenters by the resin suppliers. To investigate whether these compositional variables are important, more experiments need to be carried out on better-defined systems.

The call for lighter weight, more fuel-efficient vehicles is leading to changes in TPO composition. The weight of plastic parts can be reduced if one uses a higher modulus TPO, fabricated from a higher modulus iPP and with a semicrystalline impact modifier such as linear low-density polyethylene. This goal poses new problems. From a mechanical performance perspective, one has to be able to find compositions that provide sufficient protection against low-temperature brittle fracture. From an adhesion perspective, obtaining strong adhesion is more challenging for these high-modulus blends. In addition, one has to find adhesion promoters that provide sufficiently strong paint adhesion to meet the ever-increasing warranty requirements of the automotive industry.

To help meet this need, we have been interested in one such type of TPO composition, consisting of a relatively high molecular weight Ziegler–Natta iPP with a very low amorphous content, impact modified with a semicrystalline metallocene ethylene–butene (EB) copolymer containing 9 wt% B (EB9). We have chosen for our investigations a candidate CPO containing 20 wt% Cl. In previous publications, we examined the ability of this CPO to promote adhesion between slabs of TPO or its constituents, as measured through lap shear tests [10]. Through a combination of covalent dye labeling and laser confocal fluorescence microscopy (LCFM), we investigated aspects of the morphology of CPO-coated injection-molded plaques [11], as well as simple blends of CPO with the TPO components [12]. These studies support the idea that CPO interacts more strongly with the impact modifier (here semicrystalline EB9) than with iPP. There was a suggestion from the LCFM studies (with micrometer resolution) that the interface between CPO and EB9 was broader than that between CPO and iPP. These experiments, unfortunately, were at the resolution limit of LCFM, making it difficult to draw firm conclusions from the images.

The most important knowledge needed to design appropriately compliant systems is an understanding of the nature of the interface between CPO and injection-molded TPO. Based upon results reported in the literature, we expect that flow fields associated with the injection molding as well as the rapid crystallization at the mold wall will have an important effect on the surface structure of the TPO part. This surface structure, coupled with the processing and bake conditions used in the CPO coating process, are important factors that need to be taken into account when examining the interaction between CPO and the TPO substrate. We will return to this issue in Section 3.

High-resolution transmission electron microscopy of ultrathin sections of a polymer blend can in principle allow one to visualize directly the interfacial region between the two components. One needs a source of contrast. This can in principle be accomplished by careful selective staining of one of the components in such a way that the density observed in a TEM image is proportional to the local concentration of one of the polymer pairs. The first report describing this type of experiment with quantitative interpretation of the interface profile was that of Spontak et al. [13] who examined the mixed interface between the microphase-separated components of styrene–butadiene triblock (SBS) and diblock (SB) copolymers. This was a particularly difficult challenge, because the interfaces were estimated to be only 2–3 nm in width. They used OsO_4 vapors to stain the polybutadiene component selectively in sections ca. 30–40 nm thick. One of the most interesting conclusions from this work is that the composition of the interfacial region is not symmetric; it is enriched in S compared to B.

About five years later, Kressler et al. [14] reported similar TEM experiments on polymer blends. They used RuO_4 as a selective stain of the phenyl rings of PS in polystyrene–poly(methyl methacrylate) (PS–PMMA) blends as well as PMMA blends with a styrene–acrylonitrile (SAN-38.7) copolymer containing 38.7 wt% acrylonitrile. They comment that while one can detect the polymer concentration profile in the relatively narrow interface between PS and PMMA, the sharpness of the interface (width 5 ± 3 nm) makes it difficult to obtain detailed information with reasonable precision. They had much greater success with PMMA–SAN blends with an SAN composition just outside the miscibility window for the two polymers. These types of compositions are expected to give significant mixing in the interfacial region, and hence interfaces of sufficient width that the concentration profile can be measured by TEM with good precision. Segment density profiles were constructed from the grayscale variation across the boundary layer. From a tangent drawn at the inflection point

they determined an interfacial width of 32 ± 3 nm, and also concluded that the experimentally determined interface was asymmetric. The interfacial layer contained more SAN-38.7 than PMMA. By fitting the segment density profiles to various mathematical functions, they were able to show that the hyperbolic tangent (tan h) function proposed for polymer blends [15] and the error function (ERF) used to describe diffusion profiles [16] gave good fits to the measured profiles. In contrast, the linear profile proposed by Brochard et al. [17] did not lead to a good fit.

In this report, we describe the results of TEM measurements on the interfacial region between CPO and TPO, as well as CPO and the TPO components, iPP and EB9. The system is more complicated than that reported by Kressler et al., because iPP and EB9 are crystalline polymers. We also examine changes in the interfacial region caused by processing conditions (e.g., coating and pre-bake conditions) typical of those used in industry for the painting of plastic automotive parts. We note that Mirabella and Dioh [18] have examined cryomicrotomed sections of CPO-coated TPO plaques, using scanning transmission X-ray microscopy (STXM). Based on the STXM profiles, an interfacial thickness about 340 nm between CPO and TPO was found. This value is in the range of length scales that makes the TEM measurements of polymer blend interfaces of the sort reported by Kressler attractive, but is close to the resolution limit of STXM.

2. Experimental

2.1. Materials

Isotactic polypropylene (Escorene 1042, Ziegler–Natta catalyst) and poly(ethylene-butene) (Exact 3125, with 9 wt% butene, metallocene catalyst) copolymer were from ExxonMobil. According to Ref. [19], these polymers are characterized by $M_n = 67{,}000$ g/mol (PDI = 3.51) for iPP and $M_n = 45{,}000$ g/mol (PDI = 1.96) for EB9. Chlorinated polypropylene (CPO Superchlon 872S) with 20 wt% chlorine content was provided by Nippon Paper Chemicals Co. Ltd. By gel permeation chromatography (GPC, polystyrene standards), we determined the molecular weight of this CPO sample to be $M_w = 92{,}000$, $M_n = 41{,}000$. The anhydride content was determined by titration and found to be 0.19 mmol/g polymer [12]. As described in a previous publication [10], a sample of this polymer was functionalized with a benzothioxanthene (HY) fluorescent dye to yield a dye-labeled polymer (CPO–HY) with a maximum absorbance in the UV–vis spectrum of $\lambda_{max} = 456$ nm, and a dye content of 0.06 mmol/g. In all experiments reported here, the CPO sample contained 5 wt% of this dye-labeled polymer.

2.2. Sample preparation

The TPO_{25} blend was prepared by premixing polypropylene with 25 wt% of EB9. The mixtures were then run through a twin-screw mini-extruder (15 cm^3 capacity, DSM, The Netherlands) at 230 °C and 100 rpm on a single strand die. The TPO blend was molded into a rectangular plaque ($60.0 \times 12.6 \times 2.0$ mm) through a 2.0 mm wide pin gate using a DSM microinjection-molding machine (3.5 cm^3) at 70 psi injection pressure with a mold temperature of 43 °C. The TPO, iPP and EB9 samples were spin-coated (1000 rpm) with a solution (10 wt%) of CPO in tetrahydrofuran (THF). We use THF as the solvent to minimize solvent penetration into the plaques during the coating process. The thickness of the dry CPO layer was about 5 μm. After drying for 24 h at room temperature, some of the plaques were baked at 120 °C for 30 min to promote diffusion of CPO to the TPO substrates. Other samples were heated at 120 °C in the presence of xylene vapor. The treatment was performed in a sealed glass container. Bilayer samples (CPO/TPO) were placed on a support in the middle of a vessel that contained liquid xylene at the bottom. The container was sealed and then placed in an oven at 120 °C for 30 min.

2.3. Transmission electron microscopy (TEM)

TEM measurements were carried out at 200 kV using a Hitachi HD-2000 instrument. For the samples examined here, we obtained much better contrast in the dark-field mode, and all TEM images shown below are dark-field images. Sample sections of TPO and CPO-coated TPO were cut from the center of the plaque approximately 10 mm from the gate as shown in Scheme 1. Then ultrathin (70 nm thick) sections were obtained by cryogenically microtoming these samples on a Leica (EM FCS) microtome with a MC 1029 35° diamond knife at −140 °C. To help avoid defects or sample damage during cryosectioning, each sample was subjected to cooling for more than 2 h prior to cutting the sample at −140 °C. These sections were transferred to a carbon-coated copper grid and stained by exposure to ruthenium tetroxide (RuO_4) vapor for 30 min in a closed chamber. The composition profiles were obtained by using energy dispersive X-ray (EDX) spectroscopy analysis system. Inca software (Oxford Instruments Plc.) was used to obtain the elemental (chlorine) profiles across the interface between TPO and CPO phases, and the line profiles were collected from the TPO phase to the CPO phase as imaged in EDX mode. Line scans at three separate locations were obtained for each image. Individual EDX scans were kept to less than 30 min to minimize electron beam damage to the sample.

A reviewer asked us to comment on the possibility of sample damage during the EDX measurement, citing the work of Briber and Khoury [20] on electron energy loss spectroscopy (EELS) of polymer single crystals in TEM measurements.

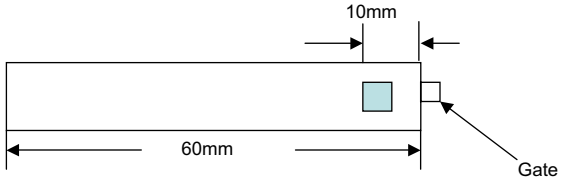

Scheme 1. Dimensions of the injection-molded plaque and the location of sample sections for TEM analysis.

These authors found a significant chlorine mass loss after relatively short exposure of poly(chlorotrifluoroethylene) single crystals to the electron beam. In our experiments, we examined thin (70 nm) sections of CPO-coated TPO. To check if the line scans led to sample damage, each section was checked by TEM imaging after each set of experiments. In some samples, with longer exposure to the electron beam, we could observe a damage line presumably due to etching of the sample. We did not observe any obvious indication of sample damage.

2.4. Differential scanning calorimetry (DSC)

A TA Q-100 DSC was used for calorimetric studies. Materials from the injection bar were heated from room temperature to 215 °C at 10 °C/min. The melting temperature was taken as the temperature corresponding to the peak in heat flow during heating. Enthalpies of crystallization and melting were obtained by integrating the heat flow curve to a flat baseline. Using the heat of fusion of a perfect iPP (207 J/g) and PE (277 J/g) [21] crystal, the weight fraction crystallinity was calculated as

$$X_c = \Delta H_m / f \Delta H_m^0 \quad (1)$$

where ΔH_m is the measured enthalpy of melting, ΔH_m^0 is the ideal enthalpy of melting a perfect crystal of polymer X, and f is the weight fraction of the polymer in the blend.

3. Results and discussion

In this study, the interfacial thickness between CPO and TPO was investigated by transmission electron microscopy (TEM) through energy dispersive X-ray (EDX) imaging. The TPO components (75 wt% iPP, 25 wt% EB9) were mixed in a mini-twin-screw extruder with a barrel temperature of 230 °C. Rectangular plaques (60.0 × 12.6 × 2.0 mm) were prepared using a microinjection-molding device through a 2.0 mm wide pin gate, with a mold temperature of 43 °C. A thin layer (5 μm) of CPO was coated onto the TPO surface. This thickness is typical of that in actual use for painted part applications, but we used tetrahydrofuran (THF) as the coating solvent to minimize solvent penetration into the TPO plaque during this part of the coating step. The CPO sample contained 5% of a sample of the material that had previously been treated to attach covalently a highly fluorescent benzothioxanthene dye. We refer to the dye-labeled sample as CPO–HY. In a previous publication, [10] we described laser confocal fluorescence microscopy (LCFM) measurements that indicated that the CPO layers applied as we describe here were flat and uniform in thickness. The presence of this small amount of dye in the CPO serves a useful function in the TEM experiments described below. CPO itself is not stained by RuO_4. Staining of the dye imparts a sufficient gray color to the CPO layer that it can be contrasted and distinguished from crystalline iPP domains, which are also not stained.

When solvent-based CPO coatings are employed in industry, one role of the solvent is to swell the surface regions of the TPO in the hopes of promoting CPO penetration into the substrate. Ryntz in particular has examined aspects of solvent penetration into TPO of different compositions, and has found that adhesion strength often correlates with the depth of solvent penetration [22]. In actual use, solvent-coated CPO is normally subjected to a pre-bake at 120 °C, below the boiling point of some of the solvent components but close to the melting temperature of EB9. In some technologies, the CPO, basecoat, and clearcoat are coated without an intervening bake, the so-called ''wet-on-wet-on-wet'' process and then subjected to a pre-bake at 120 °C before the final bake of the coating. These conditions keep the surface of the TPO in contact with aromatic solvent and solvent vapors for a significant period of time. In some of our experiments, we model this aspect of the processing conditions by placing individual CPO-coated plaques in a closed environment at 120 °C, in which they are exposed to xylene vapors. We then assess the influence of this treatment on the TPO–CPO morphology in the region of the interface.

3.1. The near-surface morphology of TPO

The near-surface morphology of an uncoated injection-molded plaque of PP/EBR9 (75/25 wt%) is shown in Fig. 1a. This ultrathin section (70 nm) was cut parallel to the injection direction at the near-gate location indicated in Scheme 1 and was stained with ruthenium tetroxide (RuO_4) vapor for 30 min before the TEM image was taken. The consistently sharp images obtained for the TPO surface, and for the TPO–CPO interface, are a good indication that little if any sample distortion occurred during the cryosectioning and staining processes. RuO_4 stains the amorphous (primarily EB9) domains of the TPO, in which the dispersed domains (EB9) appear as the brighter domains (in dark field). One can see that the EB9 domains are highly stretched along the flow direction, and exhibit a stratified morphology. Images taken in cross section (not shown) confirm that the EB9 domains are fiber like. We imagine that droplets of EB in iPP matrix were stretched by the strong shear field in the vicinity of the mold wall and trapped in place by the shear-induced crystallization of the iPP. A magnified image at surface of TPO is shown in Fig. 1b. In addition to the highly stretched EB9 domains paralleled to the surface, one can see a crystalline lamellar structure in which the lamellae are oriented perpendicular to the surface: a transcrystalline structure formed at the TPO substrate. The crystalline lamellae traverse the iPP and EB9 phases and appear to remain in registry as they cross these domains. Both Bates et al. [23] and Hiltner et al. [24] have reported this type of phenomenon previously for blends of iPP with metallocene polyethylene (mPE) copolymer. They attributed the strength of the bond between the two components to the formation of entanglements at the iPP/mPE crystal/crystal interface.

These images are qualitatively different from those reported previously in the literature for injection-molded TPO samples. Other authors have reported (see Ref. [25] for examples) that

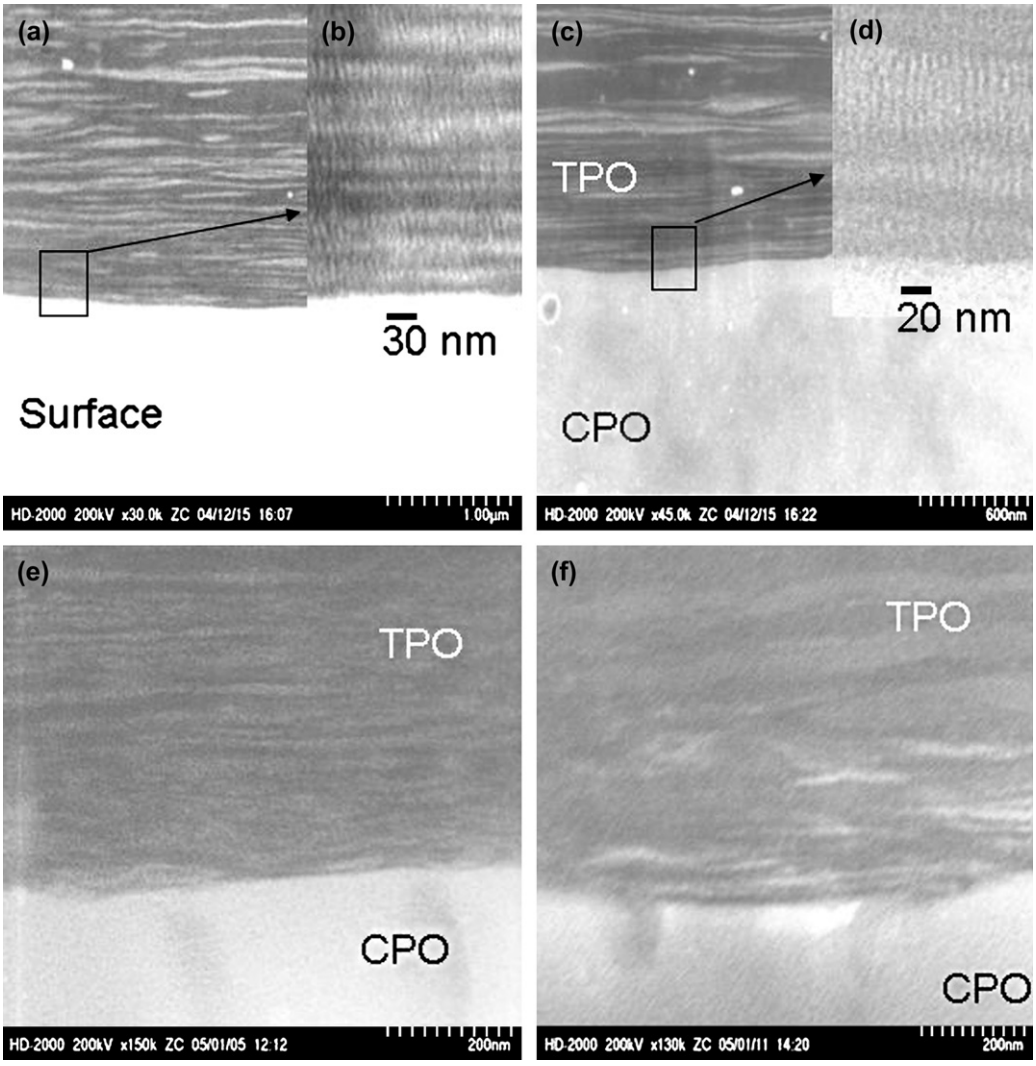

Fig. 1. Dark-field TEM images obtained with ultrathin sections after staining with RuO_4 vapor of samples taken from injection-molded plaques as shown in Scheme 1. (a, b) Near-surface region of uncoated TPO at two different magnifications. (c, d) Interfacial region of a CPO-coated TPO plaque at two different magnifications. (e) A section taken from a CPO-coated TPO plaque subjected to dry bake at 120 °C/30 min. (f) A section taken from a CPO-coated TPO plaque subjected to dry bake at 120 °C/30 min under xylene vapor.

there is a prominent PP-rich layer at the TPO surface. In Fig. 3 of Ref. [25], depicting a TEM image of an ultrathin section from a vendor-supplied plaque, this layer is well defined, largely unstained by RuO_4, and appears to be about 50 nm thick. In commenting on this image, Tang and Martin mention that the thickness of this PP-rich layer near the surface evidently depends on the processing conditions and can be varied from several hundred nanometers to several microns. Another image in Ref. [25] (Fig. 4a) shows a micrometer thick iPP rich layer at the TPO surface with a rubber-swollen layer of comparable thickness immediately beneath it. While the presence of a transcrystalline layer at the TPO surface has been reported previously, it is not seen in many samples, and this transcrystalline layer was thought to be composed exclusively of iPP [2,4].

Some of our ideas about the stretching of the EB droplets in the PP matrix and the formation of fiber-like structures are based on finding of Moffitt et al. [11], who studied the influence of laminar flow on the morphology of iPP/EB blends using LCFM in conjunction with dye-labeled EB. This model TPO blend had the same iPP used here and a similar EB content, but employed a nearly amorphous EB (EB28) containing 28 wt% butane. Their samples were pre-equilibrated in a 0.5 mm thick mold at 153 °C, below the crystallization temperature of iPP but at a temperature where the quiescent crystallization of iPP is very slow. The iPP underwent shear-induced crystallization in the near-wall regions of the mold when a short (5 s) shear pulse was applied to the sample. In those samples, the EB component in the 100 μm nearest the mold surfaces was stretched into thin fibers and then trapped in place by the rapid crystallization of the surrounding iPP matrix. While the resolution of the LCFM images (ca. 0.5 μm) is much less than that of TEM, the fibers of EB appeared to approach very close to the surface of the iPP/EB plaques formed upon cooling in the mold.

3.2. The morphology of CPO-coated TPO plaques

In Fig. 1c we present a dark-field TEM image of a CPO-coated TPO plaque without thermal treatment. As mentioned above, we used spin coating and a volatile polar solvent (THF) in the coating step to avoid as much as possible perturbation of the surface. The RuO_4-stained section shows two types of features. First one sees the pale gray color of the CPO phase that arises from staining the small amount of dye bound to this component. This staining provides a clearly visible picture of the phase boundary from the TPO substrate. One can see that the CPO/TPO interface in this as-prepared sample is very sharp on a length scale of 60 nm. In addition, one can also observe the structure internal to the TPO, which strongly resembles that seen in Fig. 1a and b. A higher magnification image of Fig. 1c is shown in Fig. 1d. Again, the transcrystalline layer is visible at the TPO surface and is unaffected by the mild coating conditions used to apply the CPO layer.

Upon close inspection of Fig. 1c, one can see a thin dark line (iPP) at the interface with CPO, with an equally thin lighter colored line on the TPO side. This observation is evidence in support of the idea that there is preferentially a thin layer of iPP at the TPO surface. Unfortunately, there is no good contrast between the stained EB and the stained CPO. Thus it would be very difficult to detect whether there is any EB in contact with the CPO layer.

To investigate the effect of baking conditions on the interfacial morphology of the CPO-coated TPO samples, we employed two different bake conditions. Under ''dry-bake'', the CPO-coated plaques were heated in an oven at 120 °C for 30 min. To model vapor exposure, another set of plaques were heated at 120 °C for 30 min in a container in which they were exposed to xylene vapor. Fig. 1e shows a dark-field TEM image of a dry baked CPO-coated TPO sample. While the interface between the TPO and the CPO is no longer as sharp as in the sample without baking, the stratified morphology of TPO substrate persists in this image, although there is somewhat less definition between the phases. The persistence of the stratified morphology in TPO substrate may be due to a confinement effect of the iPP matrix. This annealing temperature (120 °C) is above the melting temperature of EB9 (see Table 1) but well below the melting temperature of iPP. Thus the mobile, melted EBR9 phase was confined by the surrounding crystalline PP matrix; and the global features of the EB9 phase morphology was unaltered by the baking treatment. One can note that the highly stretched EBR9 domains at the interface region (within 40 nm of the outermost surface of TPO) showed distortion and broadening compared to the sample without heating (Fig. 1d). Further into the sample (>40 nm from the CPO phase), the stretched EBR9 domains remained parallel to the flow direction under the confinement of the iPP matrix.

Fig. 1f shows the corresponding dark-field TEM image of CPO-coated TPO sample baked at 120 °C for 30 min under xylene vapor. More striking changes occur in the near-surface regions of the sample. The interface is less well defined compared to the sample without exposure to xylene vapor (Fig. 1e). The EBR9 domains near the interface (within ca. 300 nm of the interface) became wider and shorter compared to the sample not exposed to xylene vapor. These effects can be explained by absorption of xylene vapor by the warm sample, partial disruption of the crystalline structure of the iPP matrix, and coalescence of EB9 droplets in the matrix. While we do not see clear evidence for the transcrystalline lamellae in the TEM images of Fig. 1e and f, we note that the skin layer, as detected by optical microscopy, persists after both the dry bake and xylene-vapor bake treatments.

The changes seen in Fig. 1f are not nearly as extreme as those inferred from images of sections obtained from fully painted plaques. For example, some of the images presented by Tang and Martin [25] show significant changes in the rubber-rich layer lying beneath the iPP-rich layer at the CPO interface, and they observe occasional droplets of the impact modifier which have diffused into the CPO layer. The Treado group [5] have also observed droplets of EP impact modifier in the CPO layer for coated plaques that they examined.

Table 1
Composition and thermal data for TPO[a] and its components

Sample[a]	iPP[b] (wt%)	EB9[b] (wt%)	T_m (°C)	ΔH (J/g) ($\Delta H/\Delta H^0$)[c]
iPP	100		165.23	90.64 (43.8%)
EB9		100	106.62	83.60 (30.18%)
TPO	75	25	165.5	65.98 (42.44%)
			106.03	16.42 (22.8%)

[a] All the samples were prepared by mini-extruder at 230 °C/100 rpm/5 min, and then injection molded at 230 °C/70 psi with mold temperature at 43 °C. Thermal data were obtained from DSC measurement at 10 °C/min from 20 to 215 °C under N_2.

[b] iPP: Escorene 1042; EB9: Exact 3125.

[c] $\Delta H^0_{PP} = 207$ J/g; $\Delta H^0_{PE} = 277$ J/g.

3.3. Probing the composition of the CPO/TPO interface

Because of the presence of Cl atoms in CPO, we can use the energy dispersive X-ray imaging (EDX) function of the TEM to probe the intermixing of CPO and non-chlorinated TPO components at the interface. In Fig. 2a we present a dark-field TEM image of a RuO_4-stained thin section of an unbaked CPO-coated TPO sample. The vertical black line through the sample, which defines the z-axis, is the coordinate from which the EDX data presented in Fig. 2b were taken. One can see that the intensity of the signal due to chlorine atoms increases from the TPO phase to the CPO phase. The magnitude of the EDX signal for chlorine in each sample was determined by reference to copper from the grid as an internal standard, but is expressed in arbitrary units. The baseline value on the TPO side of the interface was similar in intensity to the signal obtained from deep within the TPO phase. The distance scale along the z-axis has an arbitrary origin, and the important information is the width of the interface determined from the data between the two plateau regions. The transition region is located at 100–125 nm from the origin. Thus, by eye this interface appears to be ca. 25 nm wide.

Fig. 2c shows the EDX intensity profile of the chlorine element across the interface of a similar CPO-coated TPO

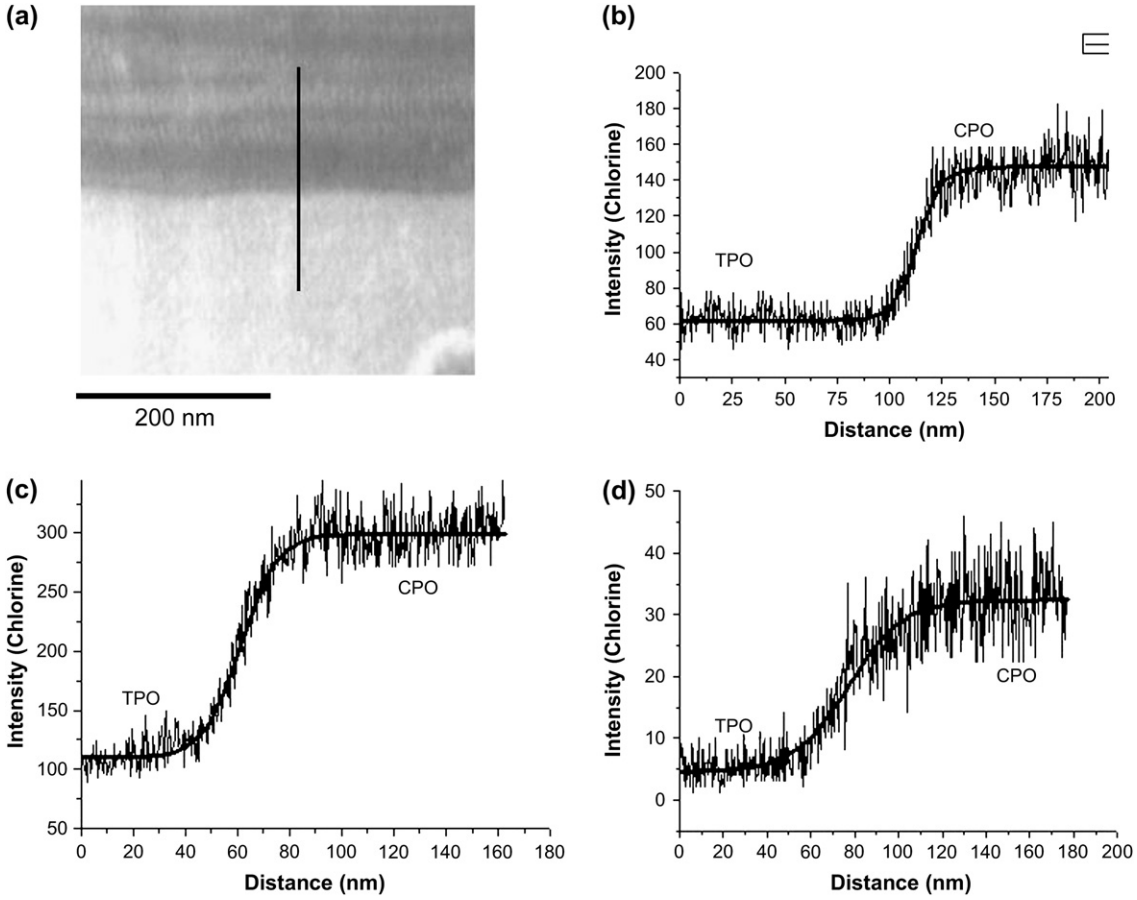

Fig. 2. TEM–EDX elemental mapping of the CPO-coated TPO samples. (a) Dark-field TEM image of CPO-coated TPO without thermal treatment. The vertical line indicates the trajectory of the EDX analysis to obtain the data shown in b. (b) The EDX line profile for chlorine across the CPO–TPO interface for a sample (see a) without thermal treatment. (c) The EDX line profile for chlorine across the CPO–TPO interface for a sample subjected to a dry bake at 120 °C/30 min. (d) The EDX line profile for chlorine across the CPO–TPO interface for a sample annealed at 120 °C/30 min under xylene vapor. The smooth lines through the data in (b)–(d) are the best fits to Eq. (1) for the composition distributions.

sample subjected to a dry bake at 120 °C for 30 min. Here the transition region is found in the range of 50–80 nm from the arbitrary origin, and the interface appears to be a bit wider than that of the sample without baking treatment. In contrast, the sample subjected to annealing in the presence of xylene vapor appears to have a much broader interface.

To obtain more quantitative information about the shapes and widths of these interface profiles, we assume that the EDX signal for Cl is proportional to the segment density $\rho(z)$ for CPO, and fitted the profiles to a hyperbolic tangent function [15]. To accommodate the arbitrary origin along the z-axis, we rewrite the theoretical Helfand expression as

$$\rho(z) = P_1 + P_2 \frac{1 \pm \tan h\left(\frac{2(z+P_3)}{\delta}\right)}{2} \tag{2}$$

where z is the distance normal to the plane of the interface taken to be centered at P_3. P_1 and P_2 are the shifts of phase position and intensity, respectively; δ is defined as the interface thickness; and the $\pm$ represents the distributions of two components across the interface. In applying Eq. (2) to fit the compositions shown in Fig. 2b and c, we treated P_i ($i = 1$–3) and δ as floating parameters. The values of interface thickness δ can then be retrieved from the fittings.

For the CPO-coated TPO sample without thermal treatment (Fig. 2b), we found a value of interface thickness at 23 ± 2.0 nm. This value broadened slightly to 28 ± 1 nm for the TPO/CPO interface subjected to dry bake at 120 °C for 30 min. The solid lines seen in Fig. 2b and c represent the best fits to Eq. (1). In both instances, the interfacial composition appears to be symmetric such that the 50% change in composition corresponds to the halfway point across the transition zone.

Fig. 2d shows the chlorine elemental intensity profile across the interface of the CPO-coated TPO sample after baking at 120 °C/30 min under xylene vapor. Two features of this plot are noteworthy. First, the transition region is substantially broader than in the samples not exposed to xylene vapor, here stretching from 50 nm to 100 nm along the z-axis. In addition, the EDX profile deviates somewhat from the tan h profile of Eq. (2). It appears that the interface is not symmetric, but is enriched in the CPO component. The width of the interface determined from the best fit of the EDX profile to Eq. (2) is 50 ± 4.0 nm. These values are collected in Table 2.

Table 2
Interface thicknesses measured from EDX data

Sample	Calculated interface thickness[a] (nm)		
TPO/CPO	21 ± 1.8[b]	23 ± 2.2	23 ± 1.7
TPO/CPO 120 °C/30 min	28 ± 1.3	29.2 ± 1.4	28.7 ± 1.8
TPO/CPO 120 °C/30 min/ xylene vapor	49.8 ± 3.9	48.7 ± 3.7	50.4 ± 4.2

[a] The three values for each sample represent values calculated for independent EDX traces across the CPO interface in an individual TEM image.
[b] The standard error of each measurement was determined from the quality of fit of the EDX trace to Eq. (2).

In order to help understand the origin of the interfacial widths seen in Fig. 2, we carried out analogous experiments on plaques prepared from the pure components of TPO: iPP and EB9. In Fig. 3a we present a dark-field TEM image of a stained thin section of CPO-coated EB9 not subjected to a bake treatment. The interface between the components seems sharp to the eye at this resolution, and the fact that the EB side of the interface is darker than the CPO side indicates that the CPO is more heavily stained in this sample. The measured EDX profile is shown in Fig. 3b. It gives an excellent fit to the tan h function, with a best-fit value of $\delta = 29 \pm 3$ nm. The result of a similar pair of experiments carried out on a CPO-coated iPP plaque, after sectioning and staining, is shown in Fig. 3c and d. Here the interface is much sharper than for CPO/EB9, and the best fit of the data to Eq. (2) yields $\delta = 15 \pm 2.0$ nm.

4. Summary and conclusions

We report transmission electron microscopy experiments that examine the nature of the interface between CPO, a chlorinated polypropylene, and a high-modulus TPO. The TPO is a blend of a relatively high molar mass isotactic polypropylene (iPP) and a semicrystalline ethylene–butene (EB) copolymer containing 9 wt% B as an impact modifier. The components were mixed in a mini-twin-screw extruder and injection molded through a pinhole gate to form rectangular plaques. By TEM, RuO_4-stained thin sections of these plaques showed a well-defined transcrystalline layer in the near-surface region.

These 2 mm thick plaques were coated with a 5 μm layer of CPO under mild conditions, and then some of the samples were subject to annealing at 120 °C for 30 min, either dry or exposed to an atmosphere saturated with xylene vapor. The xylene vapor conditions attempt to model the aromatic solvent present during the bake stage of commercial applications, where TPO parts are painted wet-on-wet-on-wet and then heated in an oven. TEM images showed that the presence of the transcrystalline layer at the CPO–TPO interface survived the dry-bake conditions, but could no longer be detected after annealing in the presence of xylene vapor.

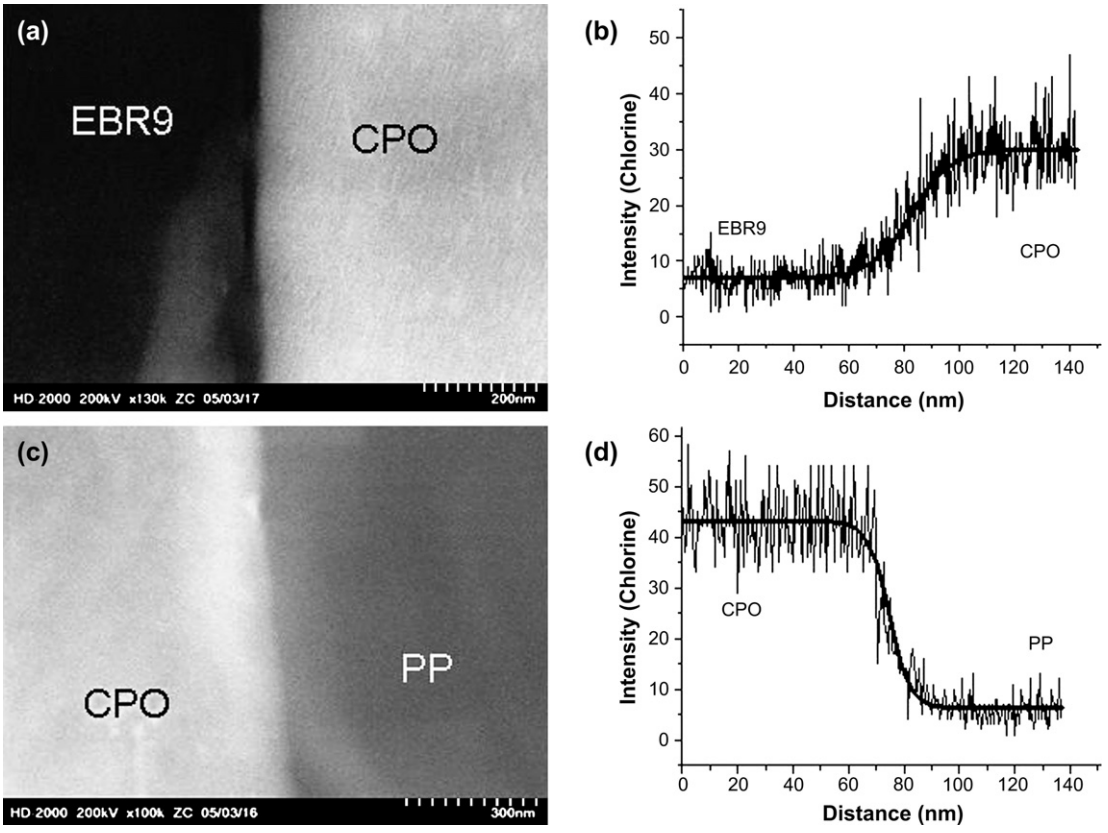

Fig. 3. TEM–EDX elemental mapping for samples of CPO-coated EB9 and CPO-coated iPP. (a) Dark-field TEM images of CPO-coated EB9 without thermal treatment. (b) The EDX line profile for chlorine across the CPO–EB interface. (c) Dark-field TEM images of CPO-coated iPP without thermal treatment. (d) The EDX line profile for chlorine across the CPO–iPP interface. The smooth lines through the data in (b) and (d) are the best fits to Eq. (1).

The presence of chlorine in the CPO made it possible to obtain the CPO segment density profile across the CPO–TPO interface using the EDX function of the high-resolution TEM instrument. For the as-prepared samples and those subjected to dry bake, the EDX profiles fit the $\tan h$ profile predicted for polymer blends by Helfand and coworkers. The widths of the interfaces fitted in this way were modestly broadened, from 23 ± 2 nm to 28 ± 1 nm, by annealing at 120 °C in the absence of solvent vapor. The xylene vapor bake had a more pronounced effect, increasing the measured interface width to 50 ± 4.0 nm. These results taken together emphasize how important the nanometer-scale near-surface organization is for these materials.

TPO itself is a blend of two components. In order to examine the nature of the interaction of CPO with the two components of the CPO, we prepared similar CPO-coated injection-molded plaques of iPP and EB9. These samples were not subjected to annealing. For iPP the annealing would be well below its melting point whereas for EB9, both components would melt and flow when heated at 120 °C. The results obtained are nonetheless very informative. We found an EB9/CPO interface width similar in magnitude (29 ± 3 nm) to that of TPO/CPO, whereas the interface for iPP/CPO was significantly narrower (15 ± 2 nm). These results support the idea that when CPO adheres to injection-molded TPO, it interacts more strongly with the impact modifier than with iPP itself.

There have been a number of attempts to try to understand the origin of this preferential interaction. For example, Ellis [9] used a group-additivity approach to estimate value of the Flory–Huggins interaction parameter χ for CPO and TPO components. He chose chlorinated PP (PP-Cl) as a model for CPO and ethylene–propylene (EP) as a model for the impact modifier. Not surprisingly, he found smaller values of χ for (PP-Cl + PP) than for (PP-Cl + EP), but he did find a narrow range of compositions (EP containing 35 wt% ethylene and a PP-Cl with 21 wt% chlorine) where the estimated interaction parameter χ (0.0058) is lower than that (0.0063) for PP + PP-Cl. From the Helfand–Tagami relationship between δ and χ, these values predict interfacial widths in the order of 10 nm for both components. This analysis assumes similar statistical segment lengths (0.8 nm) for the various polymers. We note that their analysis is consistent with our finding of a 15 nm thick interface between iPP and CPO containing 20 wt% Cl.

Acknowledgements

The authors would like to thank Nippon Paper Ind. Ltd. for kindly providing samples for this study. We also thank NESRC Canada, Visteon and E.I. DuPont Canada for financial support of this research.

References

[1] Ryntz RA, Rammurthy AC, Mihora D. J Coat Technol 1995;67(840):35–46.
[2] Ryntz RA, Xie Q, Rammurthy AC. J Coat Technol 1995;67(843):45–55.
[3] Prater TJ, Kaberline SL, Holubka JW, Ryntz RA. J Coat Technol 1996;68(857):83–9.
[4] Ryntz RA. Prog Org Coat 1996;27:241–54.
[5] (a) Morris HR, Turner JF, Munro B, Ryntz RA, Treado PJ. Langmuir 1999;15:2961–72;
(b) Morris HR, Turner JF, Munro B, Ryntz RA, Treado PJ. Langmuir 1998;14:2426–34.
[6] Schmitz PJ, Holubka JW. J Adhes 1995;48:137–48.
[7] Tomasetti E, Legras R, Heri-Mazeaud B, Nysten B. Polymer 2000;41:6597–602.
[8] Pennington BD, Ryntz RA, Urban MW. Polymer 1999;40:4795–803.
[9] Ellis TS. Polym Eng Sci 2001;41:2065–72.
[10] Yin Z, Ma Y, Chen W, Coombs N, Winnik MA, Ryntz RA, et al. Polymer 2005;46:610–23.
[11] Moffitt M, Rharbi Y, Chen W, Tong J, Winnik MA, Thurman DW, et al. J Polym Sci Part B Polym Phys 2002;40:2842–59.
[12] Ma Y, Farrinha JPS, Winnik MA, Yaneff PV, Ryntz RA. Macromolecules 2004;37:6544–52.
[13] Spontak RJ, Williams MC, Agard DA. Macromolecules 1988;21:1377–87.
[14] Kressler J, Higashida N, Inoue T, Heckmann W, Seitz F. Macromolecules 1993;26:2090–4.
[15] (a) Helfand E, Tagami Y. J Chem Phys 1971;56:3592–601;
(b) Helfand E. Acc Chem Res 1975;8:295–9;
(c) Broseta D, Fredrickson GH, Helfand E, Leibler L. Macromolecules 1990;23:132–9.
[16] Crank J. The mathematics of diffusion. 2nd ed. Oxford, UK: Oxford University Press; 1975.
[17] Brochard F, Jouffroy J, Levinson P. Macromolecules 1983;16:1638–41.
[18] Mirabella FM, Dioh NJ. Polym Eng Sci 2000;40:2000–6.
[19] Boivin KC, Barry CMF, Orroth SA. SPE ANTEC'99 1999;3:3157–61.
[20] Briber RM, Khoury F. J Polym Sci Part B Polym Phys 1998;26:621–36.
[21] Brandrup J, Immergut EH, Grulke EA. Polymer handbook. 4th ed. Interscience Publication, New York: Wiley and Sons Inc.; 1999. p. VI-6 and VI-11.
[22] Ryntz RA. J Vinyl Addit Technol 1997;3:295–300; Ryntz RA, McNeight A, Ford A. Plast Eng 1996;52(9):35–8.
[23] Chaffin KA, Bates FS, Brant P, Brown GM. J Polym Sci Part B Polym Phys 2000;38:108–21.
[24] Poon BC, Chum SP, Hiltner A, Baer E. J Appl Polym Sci 2004;92:109–15.
[25] Tang H, Martin DC. J Mater Sci 2002;37:4783–91.